Ordered aeschynite-type polar magnets RFeWO_{6} (R=Dy, Eu, Tb, and Y): A new family of type-II multiferroics

Somnath Ghara, Emmanuelle Suard, François Fauth, T. Thao Tran, P. Shiv Halasyamani, Akira Iyo, Juan Rodríguez-Carvajal, and A. Sundaresan

Phys. Rev. B **95**, 224416 — Published 13 June 2017

DOI: 10.1103/PhysRevB.95.224416

Ordered aeschynite-type polar magnets RFeWO$_6$ (R = Dy, Eu, Tb and Y): A new family of type-II multiferroics

Somnath Ghara,[1] Emmanuelle Suard,[2] Fauth Francois[3], T. Thao Tran,[4] P. Shiv Halasyamani,[4] Akira Iyo[5], J. Rodríguez-Carvajal,[2] and A. Sundaresan[1,*]

[1]*Chemistry and Physics of Materials Unit and International Centre for Materials Science, Jawaharlal Nehru Centre for Advanced Scientific Research, Jakkur P.O., Bangalore 560 064, India.*

[2]*Institut Laue-Langevin, 71, Avenue des Martyrs, CS 20156, 38042 Grenoble Cedex 9, France.*

[3]*CELLS-ALBA Synchrotron, BP1413, 08290 Cerdanyola del Vallès, Barcelona, Spain*

[4]*Department of Chemistry, University of Houston, 112 Fleming Building, Houston, TX 77204 (USA)*

[5]*NeRI, National Institute of Advanced Industrial Science and Technology, Tsukuba, Ibaraki 305-8568, Japan*

We report the discovery of magnetoelectric multiferroicity in a family of oxides, RFeWO$_6$ (R = Dy, Eu, Tb and Y) that crystallize in a polar aeschynite-type structure ($Pna2_1$) with an ordered arrangement of Fe^{3+} and W^{6+} ions. Magnetization and analysis of neutron diffraction data of DyFeWO$_6$ reveal a commensurate non-collinear antiferromagnetic ordering of Fe^{3+} spins (T_N^{Fe} ~ 18 K), which induce Dy-spins to order at the same temperature. A sudden change in electric polarization (ΔP) appears in all the compounds at the T_N^{Fe} = 15 - 18 K. The electric polarization is sensitive to applied magnetic field and the coupling between different magnetic R-ion and Fe-ion moments suppress the polarization to a different extent. While the measured polarization in polycrystalline DyFeWO$_6$ at 3.5 K is about 3 μC/m^2, the calculated value of resultant ionic polarization of the form (p_x, 0, p_z) is 75560 μC/m^2 where p_x comes from magnetic ordering and p_z is associated with the polar structure. These findings open up an avenue to explore further new polar magnets with rare-earth/transition metal ions in the ordered aeschynite-type structure.

PACS number(s): 75.85.+t, 75.50.Ee, 75.47.Lx, 61.05.fm

*E-mail: sundaresan@jncasr.ac.in

I. INTRODUCTION

Magnetoelectric multiferroics have been the subject of intense investigation in the last two decades because they not only offer new possibilities in device applications but also pose a challenge in combining electric and magnetic order in the same material [1-4]. Since the mechanism of classical ferroelectrics is antagonistic with the requirement for magnetism, several new approaches have been successful in combining these two properties in the same material [1]. Perovskites are the simplest and most investigated structure-type for multiferroic properties. The best example is the polar ($R3m$) magnetic compound, $BiFeO_3$ which shows ferroelectric ordering at T_C = 1100 K, due to polar distortion arising from the stereochemical activity of lone pair electrons of Bi^{3+} ions, and magnetism from the ordering of Fe^{3+} spins (T_N = 640 K) [5,6]. Materials belong to this class, where the long-range ordering of electric dipoles and spins occur independently at two different temperatures, are classified as type-I multiferroics [1]. On the other hand, the centrosymmetric (*Pnma*) perovskite, $TbMnO_3$ is an example for type-II multiferroics where the ferroelectricity is induced by breaking of inversion symmetry due to magnetic ordering (~ 28 K) of Mn^{3+} spins [1,7]. Since the electric polarization in this class of materials is induced by spin ordering, one can control electric polarization by a magnetic field and magnetism by an electric field, which has led to tremendous interest on type-II multiferroics [4]. Most of the type-II multiferroics are centrosymmetric in the paramagnetic state.

Recently, another kind of polar magnets have been reported to exhibit magnetoelectric and/or multiferroic properties. Unlike the polar magnets that belong to type-I multiferroics, where the polar distortion is caused by nonmagnetic ions, the non-centrosymmetric distortion in this kind of polar magnets is associated with magnetic atoms and thus they promise a strong magnetoelectric coupling. Thus, the polar magnets having their origin at the same source can

form a subclass of type-II multiferroics. For example, the polar compounds $M_2Mo_3O_8$ (M = Fe and Mn), which crystallize in hexagonal structure with space group $P6_3mc$, display electric polarization below magnetic ordering temperatures [8-10]. The interesting and promising feature of these compounds is the observation of a large linear magnetoelectric effect. Similar magnetoelectric effect is observed in another polar compound $CaBaCo_4O_7$, where a non - switchable spontaneous polarization appears below the ferrimagnetic ordering [11,12]. Collinear antiferromagnetic oxide, Ni_3TeO_6, with a polar corundum structure (space group $R3$), exhibits a non - hysteretic magnetoelectric effect [13]. Several polar corundum derivatives $A_2BB'O_6$ ($R3c$) have been reported to exhibit multiferroic properties [14-17]. Recently, a high pressure synthesized $GaFeO_3$ with partial cation ordering in the $LiNbO_3$ structure has been shown to be magnetoelectric [18].

In this article, we report magnetoelectric multiferroic properties of a family of polar magnets, RFeWO$_6$ (R = Dy, Eu, Tb and Y), which are derived from the centrosymmetric aeschynite structure by cation ordering. The most common representative oxide in aeschynite structure is $CaTa_2O_6$, which has the orthorhombic structure (*Pnma*) and consists of dimers of edge - shared $Ta^{5+}O_6$ octahedra, which are connected by corner sharing to form a three dimensional network, as shown in Figure 1c [19]. The compounds, RTiTaO$_6$ (R = La to Dy) also crystallize in the aeschynite structure, where Ti^{4+} and Ta^{5+} ions are randomly distributed in a unique crystallographic site, similar to the arrangement of $Ta^{5+}O_6$ octahedra in $CaTa_2O_6$ [20]. On the other hand, the oxides RMWO$_6$ (R = rare earth element and M = V, Cr, Fe) have been suggested to exhibit an ordered arrangement of M^{3+} and W^{6+} ions in the aeschynite structure with the polar space group $Pn2_1a$ [21]. However, the detailed structural parameters and physical properties of these oxides have not been reported so far.

From a detailed structural analysis using synchrotron and neutron diffraction data, we have confirmed that these oxides, RFeWO$_6$ with R = Dy, Eu, Tb and Y, indeed crystallize in ordered aeschynite - type structure with the polar $Pna2_1$ space group. Temperature dependent dc magnetization, neutron diffraction and heat capacity measurements reveal that these oxides exhibit a long-range antiferromagnetic ordering of Fe^{3+} - ions at $T_N^{Fe} \sim 15$ - 18 K. Observation of dielectric anomaly and electric polarization below T_N^{Fe} and their response under magnetic fields demonstrate that RFeWO$_6$ (R = Dy, Eu, Tb and Y) constitute a new family of type-II multiferroics.

II. EXPERIMENTAL DETAILS

Polycrystalline samples of RFeWO$_6$, (R = Dy, Eu and Tb) oxides were prepared by conventional solid state synthesis method through a two-step process. Firstly, the compounds RFeO$_3$ (R = Dy, Eu and Tb) were prepared by mixing stoichiometric amount of R_2O_3, (R = Dy and Eu) or Tb_4O_7 with Fe_2O_3, and heating at the final temperature of 1350 °C for 24 hr in air with several intermittent grindings. All the rare earth oxides were preheated at 900 °C for 12 hr in air before use. In the second step, RFeO$_3$ and WO$_3$ were mixed stoichiometrically and the mixtures were heated at final temperatures of 1020 °C, 1110 °C and 1060 °C for 12 hr in pure argon atmosphere for R = Dy, Eu and Tb, respectively. YFeWO$_6$ was prepared at high pressure (4.5 Gpa) and high temperature (1000 °C) using a multi anvil cubic high-pressure apparatus from the starting materials, Y_2O_3, Fe_2O_3 and WO$_3$.

Room temperature synchrotron X - ray diffraction data for all the samples were collected at the Materials Science Powder Diffraction beamline (BL04 - MSPD) of the ALBA synchrotron facility at Barcelona, Spain using the wavelengths , λ = 0.3544 and 0.3171Å [22,23]. Additional data were also collected at low temperatures for DyFeWO$_6$. Neutron diffraction data were

recorded on $DyFeWO_6$ on D2B diffractometer at the Institut Laue - Langevin (ILL, Grenoble, France) with a wavelength of λ = 1.594 Å at all temperatures. Room temperature neutron diffraction data on $TbFeWO_6$ were also collected with the same wavelength on D2B diffractometer. Room temperature powder second harmonic generation (SHG) measurements were performed on $DyFeWO_6$ and $EuFeWO_6$ using a modified Kurtz - NLO system with a pulsed Nd:YAG laser (λ = 1064 nm). The details of equipment and methodology have already been reported [24-26].

DC magnetization measurements were carried out with a Superconducting Quantum Interference Device (SQUID, Quantum Design - USA). Temperature dependent magnetization was measured under field - cooled (FC) condition, where the sample was cooled under a magnetic field of 100 Oe and the data was recorded during heating with a rate of 3 K/min. Magnetic field dependent magnetization measurements at fixed temperatures were carried out with stable at each field mode. Heat capacity was measured in a Physical Properties Measurement System (PPMS, Quantum Design) using a relaxation technique. Temperature dependent dielectric constant was measured under different frequency and various applied magnetic fields with an Agilent E4980A LCR meter with 2 K/min rate. Pyroelectric current was measured with a Keithley 6517A electrometer. In pyroelectric current measurements, the sample was cooled across the magnetic ordering temperature with an electric field and then shorted for 45 min to remove stray charges and then the current was recorded during heating with a rate of 10 K/min. PPMS was used for temperature and magnetic field dependent dielectric and pyroelectric current measurements with the help of a multifunctional probe provided by Quantum Design. For dc - biased current measurements, the sample was cooled to lowest temperature without any poling field. At lowest temperature, the dc electric field was applied and the current was recorded while warming the

sample with a rate of 10 K/min under the electric field [27]. For all electrical measurements, contacts were made on sintered pellet samples with a high performance silver paste from Ted Pella, Inc.

III. RESULTS AND DISCUSSION

In this section, first we present detailed analysis of crystal and magnetic structures and results of multiferroicity in $DyFeWO_6$. Then, we discuss the experimental results in other oxides, $RFeWO_6$ (R = Eu, Tb and Y).

A. $DyFeWO_6$

To determine crystal structure at room temperature, the synchrotron powder X - ray diffraction pattern of $DyFeWO_6$ was indexed with DICVOL program available in the FullProf Suite [28]. The reflection conditions obtained from indexing are: $0kl$: $k + l = 2n$, $hk0$: $h = 2n$, which suggest that the most probable space groups could be either $Pnma$ or $Pn2_1a$. Since the reflection condition for both of these space groups is same, it is not possible to conclude the real space group using diffraction data. However, $Pnma$ is centrosymmetric, while $Pn2_1a$ is a polar space group. SHG measurements revealed that this material is SHG active with efficiency comparable to that of α-SiO_2 supporting the polar space group $Pn2_1a$. Therefore, to determine the complete structure, we have performed a combined Rietveld refinement analysis of the room temperature synchrotron X - ray and neutron diffraction data using FullProf software. In this process, we have used the standard setting of $Pna2_1$ (space group no. 33) instead of the non-standard $Pn2_1a$ setting. Since the atomic positions are not known and $Pna2_1$ is a subgroup of $Pnam$ (another setting of $Pnma$), the atomic positions in $CaTa_2O_6$ in $Pnma$ space group have been used and converted from $Pnma$ to $Pna2_1$ space group using SUBGROUPGRAPH and TRANSTRU program available in Bilbao Crystallographic Server [29]. The refined synchrotron X - ray and

neutron diffraction patterns are shown in Figure 1a and b, respectively and the obtained crystal structure of $DyFeWO_6$ is displayed in Figure 1d. The detailed structural parameters obtained from the refinements are given in Table-I. It is observed that the 8*d* octahedral site in centrosymmetric *Pnam* structure (Figure 1c) of $CaTa_2O_6$ splits into two 4*a* octahedral sites in $Pna2_1$, where Fe^{3+} and W^{6+} ions are arranged in an ordered manner. The cation ordering occurs because of the size and charge differences between Fe^{3+} and W^{6+} ions. $Fe^{3+}O_6$ and $W^{6+}O_6$ octahedra form edge-shared dimers which are connected through corner sharing to form a three dimensional structure. The selected bond lengths obtained from refinement are shown in Table-II. The average <Dy-O>, <Fe-O> and <W-O> bond lengths, 2.38, 2.00, and 1.94 Å, respectively are consistent with those reported in $DyFeO_3$ and $MnWO_4$, indicating Dy^{3+}, Fe^{3+} and W^{6+} oxidation states [30,31]. Further, the results of bond valence sum calculations, as shown in Table-II, confirm the +3 and +6 oxidation state of Dy/Fe and W ions, respectively.

Figure 2a shows temperature dependence of magnetization data, M (T), measured with an applied field of 100 Oe under field - cooled (FC) condition. A clear hump - like anomaly in M (T) and the sharp λ - anomaly in the heat capacity, C_P (T) seen at 18 K, as seen in Figure 2b, indicate the long - range antiferromagnetic ordering of Fe^{3+} spins. Upon further cooling, M (T) increases and exhibits a broad maximum around 12 K. At 5 K, there is a step in M (T) data indicating a long - range cooperative antiferromagnetic ordering of Dy^{3+} moments. Indeed, as discussed later, our neutron diffraction results reveal that the Fe^{3+} ordered moments induce Dy^{3+} moments to order with the same propagation vector at 18 K. Because of this, we do not find any anomaly in C_P (T) at the independent ordering temperature (5 K) of Dy^{3+} moments. Temperature dependent inverse susceptibility ($1/\chi_{mol}$) *vs.* temperature data could be fitted with Curie - Weiss law at higher temperatures (not shown). The obtained effective paramagnetic moment (μ_{eff}) is

12.5 μ_B/f.u., which is close to the theoretical moment (12.17 μ_B/f.u.) for Dy^{3+} and Fe^{3+} moments. The Curie - Weiss temperature (θ_{CW}) obtained from the fit is - 21 K. This is consistent with the observed antiferromagnetic ordering at 18 K. Magnetic field dependent magnetization *M* (*H*) at different temperatures are shown in the inset of Figure 2a. The *M* (*H*) curve at 15 K is consistent with the antiferromagnetic behavior. However, at 2 K, the *M* (*H*) data exhibit field - induced step indicating the meta-magnetic nature of Dy^{3+} magnetism. Above 18 K, the *M* (*H*) curve resembles paramagnetic behavior.

In order to understand the magnetization behavior and determine the magnetic structure, low temperature neutron diffraction data have been analyzed. In Figure 3a, the neutron diffraction pattern recorded at 3.5 K is shown, where Rietveld refinement has been performed including magnetic and nuclear structure model. The magnetic structure has been solved using symmetry analysis with both BasIreps (FullProf Suite) and MAXMAGN (Bilbao Crystallographic Server) programs [32]. BasIreps provides a complex 2-D irreducible representation that is transformed to real using Physically Irreducible Representations from the table of B. Campbell and H. Stokes. The 12 basis functions obtained indicate that we have to impose special directions in the representation space (put constraints in the coefficients) in order to get more symmetric magnetic structures, otherwise we obtain triclinic structures. Using MAXMAGN, we obtain three maximal magnetic space groups compatible with the propagation vector **k** = (0, 1/2, 1/2), these are: C_ac, P_ac and P_S1. The magnetic space group C_ac describes correctly the diffraction pattern and corresponds to a particular selection of basis vectors obtained with BasIreps. Using the Belov-Neronova-Smirnova (BNS) notation, the transformation from the setting we use, related to the paramagnetic basis as (**a**, 2**b**, 2**c**; 0, 0, 0), to the standard BNS cell is (-**c**, **b**, **a**; 0, 1/8, 0), so the **b** - axis is kept and the glide plane *c* of C_ac is the original glide plane *a* perpendicular to the **b** -

axis of $Pna2_1$ [33]. We have used the formalism of propagation vectors by using the crystallographic unit cell as the basis for the describing the magnetic structure and replacing the anti-translations and centering translations of the magnetic structure when described in the magnetic unit cell by the effect of the propagation vector. The small metric distortion due to the reduction of symmetry to monoclinic cannot be detected with the resolution of the present neutron and synchrotron measurements. Only an anomaly in the evolution of the cell parameters as a function of temperature can clearly be seen at T_N^{Fe} in the synchrotron data (not shown). However, very small changes in the intensities of Bragg reflection may contain information about the distortion of the crystal structure. We have used a recently implemented option in FullProf that allows to combine crystallographic and magnetic symmetry modes in order to determine the structural changes accompanying the magnetic ordering (discussed later) [34]. From the point of view of symmetry, the magnetic point group derived from C_ac is $m1'$, with m perpendicular to the **b** - axis of the paramagnetic space group and therefore the macroscopic properties in the magnetically ordered phase are driven by this group. The allowed electric polarization is constrained to be within the m - plane, so that in the magnetic phase the polarization should be of the form $\mathbf{P}_m = (p_x, 0, p_z)$. The paramagnetic group $Pna2_11'$ is already polar and the allowed polarization, even if it is not detected experimentally, is of the form $\mathbf{P} = (0, 0, p_z)$, so in the magnetic phase a new component is allowed.

We observe a very unusual behavior of Dy^{3+} - magnetism in this compound. If we do not consider Dy^{3+} moment in refining 15 K data, we could refine the pattern, but the magnetic moment of Fe^{3+} becomes 5.7 μ_B which is too high. This implies that there should be a contribution of Dy^{3+} moments at 15 K probably induced by the ordering of Fe-spins. In order to confirm this, we refined the neutron data at 15, 10 and 3.5 K, including Dy-contribution with the

same propagation vector of Fe-spins. This model gave a best fit to the data with good reliability parameters and the obtained magnetic moments of Fe^{3+} and Dy^{3+} ions are given in Table-III, where the crystallographic parameters at 3.5 K are also shown.

The obtained magnetic structure at 3.5 K is shown at Figure 3b. It is interesting to note the unusual arrangement of both Fe and Dy spins in this compound. There are two different Fe spin sites. In each site, the spins are aligned antiferromagnetically but between the sites (along the *a*-axis) they are nearly perpendicular to each other and thus the structure is strongly non-collinear. Similar non-collinear arrangement of Dy spins is observed with a tendency to get nearly perpendicular Dy^{3+} moments at low temperature. This could be due to the single - ion anisotropy of Dy^{3+} ions. We found that the magnetic structure remains same in the temperature range between 3.5 K and 18 K despite the independent magnetic correlations develop among Dy^{3+} spins below 5 K. The magnetic structure is essentially non-centrosymmetric as the underlying crystal structure is polar. This kind of magnetic structure is very unusual and a model to explain the observed spin configuration still needs to be elaborated and the detailed description of the observed magnetic structure will be published elsewhere.

Temperature dependence of the real part of dielectric constant $\varepsilon'(T)$ measured with different frequencies is shown in Figure 4a. A clear peak is observed around magnetic ordering temperature T_N^{Fe} = 18 K in $\varepsilon'(T)$, which is associated with a peak in the imaginary part of dielectric constant $\varepsilon''(T)$ (shown in the inset of Figure 4a). These peaks in $\varepsilon'(T)$ and $\varepsilon''(T)$ around T_N^{Fe} do not shift with increasing frequency, which indicates that these are not associated with any relaxation phenomenon. However, another broad peak is found in $\varepsilon''(T)$ at further lower temperature, which shifts to higher temperature with increasing frequency, indicating that

it is associated with intrinsic dielectric relaxation of the material. Note that the value of dielectric loss ($tan\,\delta = \frac{\varepsilon''}{\varepsilon'}$) is very small (~ 0.02) at 50 kHz around T_N^{Fe}, which suggests that the compound is highly insulating at low temperature. Thus, the occurrence of dielectric anomaly at the magnetic ordering temperature indicates a close correlation between magnetic and dielectric properties. This correlation is further confirmed from temperature dependent dielectric constant measured with 50 kHz under different magnetic fields (Figure 4b). The magnetic field strongly suppresses the anomaly around T_N^{Fe} in $\varepsilon'(T)$. At further lower temperature, $\varepsilon'(T)$ increases with increasing magnetic field, indicating possible field induced change in magnetic structure of Dy^{3+} spins. Thus, Figure 4a and b confirm that a strong magnetodielectric effect is present below T_N^{Fe} in the present system.

To investigate whether the dielectric anomaly is associated with appearance of electric polarization, pyroelectric current was measured with an applied electric field of $E = \pm 9.2$ kV/cm and different applied magnetic fields. The electric polarization ΔP (T) obtained by integrating the pyroelectric current with measurement duration is displayed in Figure 5a. The presence of sharp asymmetric pyroelectric current peak at zero - magnetic field indicates the appearance of electric polarization below T_N^{Fe}. Since this compounds has a polar structure, there can be a non - zero electric polarization (p_z) above T_N^{Fe}. However, we could not find measurable polarization in the paramagnetic region, indicating that this compound is only pyroelectric or the switchable polarization too small to be measured. The observed electric polarization below T_N^{Fe} is the result of possible enhancement of the high temperature electric polarization (p_z) and emergence of the new component p_x due to magnetic ordering of Fe^{3+} ions as discussed above. It can be seen from the Figure 5a, that the electric polarization is also affected by the external magnetic field, as

observed in ε' (T) in Figure 4c, and vanished under a magnetic field of 40 kOe. In the inset of Figure 5a, magnetic field dependent electric polarization measured at 10 K is shown and it clearly demonstrates the suppression of electric polarization under applied magnetic field. Thus, the presence of dielectric anomaly and electric polarization below $T_{\mathrm{N}}^{\mathrm{Fe}}$ and their response under magnetic field suggest that the present compound is a magnetoelectric multiferroic or type-II multiferroic. However the magnetic point group $m1'$ forbids the first order magnetoelectric effect, so only the second order inverse magnetoelectric tensor ($P_i = \alpha_{ijk}^{T} H_j H_k$) is allowed. Though the pyroelectric current can be switched in polycrystalline sample by applying opposite poling electric field (Figure 5a), it requires single crystal study to confirm the polarization switching.

In order to confirm that the observed pyroelectric current peak near $T_{\mathrm{N}}^{\mathrm{Fe}}$ is due to depolarization current associated with electric dipoles and not due to thermally stimulated free charge carriers, we measured dc-biased current which can distinguish these two different origin as reported, where current was recorded with increasing temperature in the presence of applied dc - electric field without any pre-poling [27]. In Figure 5b, the temperature dependent dc-biased current measured under an applied electric field, E_{dc} = + 9.2 kV/cm is shown. The dc-biased current exhibits a broad upward and then a sharp downward peak with increasing temperature. The upward broad peak is associated with the polarization of the material which slowly increases with increasing temperature in the presence of electric field. The downward peak around $T_{\mathrm{N}}^{\mathrm{Fe}}$ indicates the depolarization of the polarized dipoles. A small positive shift could be due to higher warming rate (10 K/min), which is an important parameter in this measurement. These results confirm the intrinsic nature of the electric polarization. Further, the absence of any feature

associated with dc-biased current measured with a magnetic field of 40 kOe (Figure 5b) supports the suppression of electric polarization by magnetic field.

Using the approach of symmetry modes, we have refined the most relevant structural modes amplitudes in order to determine what is the most important structural change accompanying the magnetic ordering [34]. There are two active representations of the paramagnetic group $Pna2_11'$ for structural distortions, GM1 and GM4, and the global refined amplitudes for both representations are: A_GM1= 0.04(1) Å and A_GM4= 0.17(8) Å, the most important displacements correspond to the parent O2, O4, and O6 (which are split into two independent atoms each) with approximate displacements of 0.035 Å/atom with respect to the paramagnetic phase.

A calculation of the ionic polarization in the paramagnetic polar phase at 30 K gives a value of 6300 $\mu C/m^2$ along the **c** - axis, which arises due to a shift of barycenter of the positive and negative charges by 0.0034 Å [35]. Though this value of polarization is measurable experimentally, we could not find any polarization because of the fact that there is no polar-nonpolar phase transition in the accessible temperature range and the polycrystalline nature of the sample. On the contrary, the same calculation in the magnetic state (3.5 K) using the resulting crystal structure from the refinement of the symmetry - mode amplitudes gives a value of an order of magnitude greater: 75,560 $\mu C/m^2$ with $\mathbf{P} \approx (-62{,}200, 0, 42{,}900)\ \mu C/m^2$. However, the low value of polarization obtained from pyroelectric current measurements could be due to the polycrystalline nature of the sample.

B. $EuFeWO_6$

The ordered aeschynite-type polar crystal structure (space group $Pna2_1$) of $EuFeWO_6$ is confirmed by the Rietveld refinement of room temperature synchrotron X - ray diffraction data (shown in Figure S1 in the Supplemental Material) and room temperature SHG measurement [36]. The structural parameters obtained from refinement are given in Table - S1 in the Supplemental Material [36]. In Figure 6a, the temperature dependent magnetization, M (T) shows a peak around 17 K indicating the magnetic ordering of Fe^{3+} - ions. The long - range magnetic ordering is confirmed by a sharp λ - type anomaly in C_P (T), as shown in Figure 6b. M (H) loop at 2 K is consistent with antiferromagnetic ordering (see the inset of Figure 6a). Curie - Weiss fit to susceptibility data at high temperatures suggests that Eu^{3+} contributes to the effective paramagnetic moment, but it does not order down to 2 K as suggested by M (T) and C_P (T). The paramagnetic nature of Eu^{3+} - moments is consistent with the increase in M (T) at low temperatures. A sharp dielectric anomaly is observed around T_N^{Fe} (Figure 6c), which seems to be smeared out under magnetic field. Electric polarization is observed below T_N^{Fe} in zero magnetic field as shown in Figure 6d and it is suppressed with increasing magnetic field. These results suggest that $EuFeWO_6$ is also a type - II multiferroic. Unlike $DyFeWO_6$, the electric polarization in $EuFeWO_6$ is suppressed at relatively large magnetic field (80 kOe).

C. $TbFeWO_6$

Results of combined Rietveld refinement of room temperature synchrotron X-ray and neutron diffraction data of $TbFeWO_6$ are shown in Figure S2 in the Supplemental Material and the structural parameters are given in Table - S2 [36]. Temperature dependent field - cooled (FC) magnetization M (T) measured under a magnetic field of 100 Oe is shown in Figure 7a, where a

sharp peak is observed at 2.4 K. Heat capacity data C_P (T) exhibits two sharp λ - kind anomaly around 15 K and 2.4 K (Figure 7b), suggesting long - range antiferromagnetic ordering of Fe^{3+} and Tb^{3+} spins, respectively. Because of relatively large paramagnetic moment of Tb^{3+} ions, there is no anomaly in M (T) around the Fe-ordering temperature (T_N^{Fe} ~ 15 K). Unlike $DyFeWO_6$, where the Dy-moments are induced to order at T_N^{Fe}, the observation of anomaly in C_P (T) at T_N^{Tb} ~ 2.4 K suggest that Tb^{3+} moments remain paramagnetic above T_N^{Tb} ~ 2.4 K. However, low temperature neutron diffraction measurements are required to confirm this suggestion. Magnetic field dependent magnetization, M (H) data (see the inset of Figure 7a) suggest antiferromagnetic behavior below T_N^{Fe} ~ 15 K and a meta-magnetic behavior at 2 K due to field induced changes associated with Tb^{3+} ordering. In Figure 7c, temperature dependent real part of dielectric constant ε' (T) measured with 50 kHz under different magnetic fields are shown. In zero - magnetic field, two sharp dielectric anomalies are observed around T_N^{Fe} ~ 15 K and T_N^{Tb} ~ 2.4 K. The anomaly around T_N^{Fe} is suppressed and becomes broad under high magnetic field, while the anomaly around T_N^{Tb} is vanished in high magnetic field. Temperature dependence of electric polarization, ΔP (T), is shown in Figure 7d where the appearance of non - zero electric polarization below T_N^{Fe} ~ 15 K in zero - magnetic field, suggests the presence of multiferroicity in $TbFeWO_6$. The electric polarization is vanished under an applied magnetic field of 10 kOe, which indicates that a strong magnetoelectric effect is present below T_N^{Fe} ~ 15 K.

D. $YFeWO_6$

Synchrotron X - ray diffraction pattern of $YFeWO_6$ and the structural parameters obtained at the final Rietveld refinement are given in Figure S3 and Table - S3, respectively in the Supplemental Material [36]. M (T) and C_P (T) data are shown in Figure 8a and b, respectively and M (H) data is

given in the inset of Figure 8a. A peak observed around 15 K in both of the M (T) and C_P (T) data and the linear behavior of M (H) loop at 2 K suggest antiferromagnetic ordering of Fe^{3+} moments around $T_N^{Fe} \sim 15$ K. In $\varepsilon'(T)$ data (Figure 8c), a sharp anomaly is observed in zero - magnetic field around T_N^{Fe} and it is not affected under applied magnetic fields but shifts slightly to a lower temperature at 80 kOe. ΔP (T) data measured with different magnetic fields are shown in Figure 8d. Similar to other compounds, electric polarization appears below T_N^{Fe} and its magnitude decreases with applied magnetic fields. However, unlike the magnetic R-ions, the electric polarization in $YFeWO_6$ does not vanish even at 80 kOe. The fact that, the observation of electric polarization below $T_N^{Fe} \sim 15$ K in $YFeWO_6$ indicates that the emergence of electric polarization in $RFeWO_6$ is solely due to the long - range magnetic ordering of Fe^{3+} moments. The R-ion moments only affect the polarization through the coupling between R- and Fe-spins. It should be mentioned here that all these samples exhibit switchable electric polarization under a negative electric field. Though we have not determined magnetic structure in compounds other than $DyFeWO_6$, the appearance of electric polarization at T_N^{Fe} indicates that all the compounds should have a similar magnetic structure of Fe-spins.

IV. CONCLUSION

In conclusion, we have demonstrated magnetoelectric multiferroic properties in a family of oxides $RFeWO_6$ (R = Dy, Eu, Tb and Y), which belong to a polar aeschynite - type structure. A new kind of unusual commensurate and non-collinear magnetic structure of Fe^{3+} spins is responsible for enhancing the electric polarization below the magnetic ordering temperature. The magnetic coupling between R and Fe-ions has a strong effect on the electric polarization. It requires further studies to understand the mechanism of polarization associated with magnetic

ordering and the effect of coupling between *R*- and Fe-spins on the electric polarization. Finding magnetoelectric properties in this class of compounds opens up an avenue for exploring new polar magnets with high magnetic ordering temperature.

Acknowledgments

AS and SG thank the Department of Science and Technology, India (SR/NM/Z-07/2015) for the financial support for performing synchrotron X - ray diffraction experiments at ALBA, Barcelona, Spain and Jawaharlal Nehru Centre for Advanced Scientific Research (JNCASR) for managing the project. A. S. and S. G. acknowledge Sheikh Saqr Laboratory at Jawaharlal Nehru Centre for Advanced Scientific Research for providing experimental facilities. S. G. acknowledges Jawaharlal Nehru Centre for Advanced Scientific Research for providing a research fellowship. PSH and TTT thank the Welch Foundation (Grant E-1457) and the NSF-DMR-1503573 for support.

References:

[1] D. Khomskii, Trend: Classifying multiferroics: Mechanisms and effects, Physics **2,** 20 (2009).

[2] W. Eerenstein, N. Mathur, and J. F. Scott, Multiferroic and magnetoelectric materials, Nature **442,** 759 (2006).

[3] S.-W. Cheong and M. Mostovoy, Multiferroics: a magnetic twist for ferroelectricity, Nat. Mater. **6,** 13 (2007).

[4] Y. Tokura, S. Seki, and N. Nagaosa, Multiferroics of spin origin, Rep. Prog. Phys. **77,** 076501 (2014).

[5] G. Smolenskiĭ and I. Chupis, Ferroelectromagnets, Soviet Physics Uspekhi **25,** 475 (1982).

[6] J. Wang, J. Neaton, H. Zheng, V. Nagarajan, S. Ogale, B. Liu, D. Viehland, V. Vaithyanathan, D. Schlom, and U. Waghmare, Epitaxial $BiFeO_3$ multiferroic thin film heterostructures, Science **299,** 1719 (2003).

[7] T. Kimura, T. Goto, H. Shintani, K. Ishizaka, T. Arima, and Y. Tokura, Magnetic control of ferroelectric polarization, Nature **426,** 55 (2003).

[8] Y. Wang, G. L. Pascut, B. Gao, T. A. Tyson, K. Haule, V. Kiryukhin, and S.-W. Cheong, Unveiling hidden ferrimagnetism and giant magnetoelectricity in polar magnet $Fe_2Mo_3O_8$, Sci. Rep. **5**, 12268; doi: 10.1038/srep12268 (2015).

[9] T. Kurumaji, S. Ishiwata, and Y. Tokura, Doping-Tunable Ferrimagnetic Phase with Large Linear Magnetoelectric Effect in a Polar Magnet $Fe_2Mo_3O_8$, Phys. Rev. X **5,** 031034 (2015).

[10] T. Kurumaji, S. Ishiwata, and Y. Tokura, Diagonal magnetoelectric susceptibility and effect of Fe doping in the polar ferrimagnet $Mn_2Mo_3O_8$, Phys. Rev. B **95,** 045142 (2017).

[11] V. Caignaert, A. Maignan, K. Singh, C. Simon, V. Pralong, B. Raveau, J. F. Mitchell, H. Zheng, A. Huq, and L. Chapon, Gigantic magnetic-field-induced polarization and magnetoelectric coupling in a ferrimagnetic oxide $CaBaCo_4O_7$, Phys. Rev. B **88,** 174403 (2013).

[12] R. Johnson, K. Cao, F. Giustino, and P. Radaelli, $CaBaCo_4O_7$: A ferrimagnetic pyroelectric, Phys. Rev. B **90,** 045129 (2014).

[13] Y. S. Oh, S. Artyukhin, J. J. Yang, V. Zapf, J. W. Kim, D. Vanderbilt, and S.-W. Cheong, Non-hysteretic colossal magnetoelectricity in a collinear antiferromagnet, Nat. Commun. **5,** 3201 (2014).

[14] M. R. Li, D. Walker, M. Retuerto, T. Sarkar, J. Hadermann, P. W. Stephens, M. Croft, A. Ignatov, C. P. Grams, and J. Hemberger, Polar and Magnetic Mn_2FeMO_6 (M = Nb, Ta) with $LiNbO_3$-type Structure: High-Pressure Synthesis, Angew. Chem. Int. Ed. **52,** 8406 (2013).

[15] M.-R. Li, P. W. Stephens, M. Retuerto, T. Sarkar, C. P. Grams, J. Hemberger, M. C. Croft, D. Walker, and M. Greenblatt, Designing polar and magnetic oxides: Zn_2FeTaO_6-in search of multiferroics, J. Am. Chem. Soc. **136,** 8508 (2014).

[16] M. R. Li, M. Retuerto, D. Walker, T. Sarkar, P. W. Stephens, S. Mukherjee, T. S. Dasgupta, J. P. Hodges, M. Croft, and C. P. Grams, Magnetic-Structure-Stabilized Polarization in an Above-Room-Temperature Ferrimagnet, Angew. Chem. Int. Ed. **53,** 10774 (2014).

[17] M. R. Li, M. Croft, P. W. Stephens, M. Ye, D. Vanderbilt, M. Retuerto, Z. Deng, C. P. Grams, J. Hemberger, and J. Hadermann, Mn_2FeWO_6: A New Ni_3TeO_6-Type Polar and Magnetic Oxide, Adv. Mater. **27,** 2177 (2015).

[18] H. Niu, M. J. Pitcher, A. J. Corkett, S. Ling, P. Mandal, M. Zanella, K. Dawson, P. Stamenov, D. Batuk, A. M. Abakumov, C. L. Bull, R. I. Smith, C. A. Murray, S. J. Day, B. Slater, F. Cora, J. B. Claridge, and M. J. Rosseinsky, Room Temperature Magnetically Ordered Polar Corundum $GaFeO_3$ Displaying Magnetoelectric Coupling, J. Am. Chem. Soc. **139,** 1520 (2017).

[19] L. Jahnberg, Crystal structure of orthorhombic $CaTa_2O_6$, Acta Chem. Scand. **71,** 2548 (1963).

[20] G. J. Thorogood, M. Avdeev, and B. J. Kennedy, Structural studies of the aeschynite–euxenite transformation in the series $Ln(TiTa)O_6$ Ln = Lanthanide, Solid State Sci **12,** 1263 (2010).

[21] R. Salmon, H. Baudry, J. Grannec, and G. Le Flem, Sur de nouvelles séries de composés du tungsten +IV de type aeschynite, Revue de Chimie Minerale **11,** 71 (1974).

[22] F. Fauth, I. Peral, C. Popescu, and M. Knapp, The new material science powder diffraction beamline at ALBA synchrotron, Powder Diffraction **28,** S360 (2013).

[23] F. Fauth, R. Boer, F. Gil-Ortiz, C. Popescu, O. Vallcorba, I. Peral, D. Fullà, J. Benach, and J. Juanhuix, The crystallography stations at the Alba synchrotron, The European Physical Journal Plus **130,** 160 (2015).

[24] S. Kurtz and T. Perry, A powder technique for the evaluation of nonlinear optical materials, J. Appl. Phys. **39,** 3798 (1968).

[25] K. E. Rieckhoff and W. L. Peticolas, Optical second-harmonic generation in crystalline amino acids, Science **147,** 610 (1965).

[26] K. M. Ok, E. O. Chi, and P. S. Halasyamani, Bulk characterization methods for non-centrosymmetric materials: second-harmonic generation, piezoelectricity, pyroelectricity, and ferroelectricity, Chem. Soc. Rev. **35,** 710 (2006).

[27] C. De, S. Ghara, and A. Sundaresan, Effect of internal electric field on ferroelectric polarization in multiferroic $TbMnO_3$, Solid State Commun. **205,** 61 (2015).

[28] J. Rodriguez-Carvajal, in *FULLPROF: a program for Rietveld refinement and pattern matching analysis*, 1990 (Toulouse, France:[sn]).

[29] S. Ivantchev, E. Kroumova, G. Madariaga, J. Perez-Mato, and M. Aroyo, SUBGROUPGRAPH: a computer program for analysis of group–subgroup relations between space groups, J. Appl. Crystallogr. **33,** 1190 (2000).

[30] V. A. Streltsov and N. Ishizawa, Synchrotron X-ray study of the electron density in $RFeO_3$ (R = Nd, Dy), Acta Crystallographica Section B: Structural Science **55,** 1 (1999).

[31] A. Kuzmin and J. Purans, Local atomic and electronic structure of tungsten ions in AWO_4 crystals of scheelite and wolframite types, Radiation measurements **33,** 583 (2001).

[32] J. Perez-Mato, S. Gallego, E. Tasci, L. Elcoro, G. de la Flor, and M. Aroyo, Symmetry-based computational tools for magnetic crystallography, Annual Review of Materials Research **45,** 217 (2015).

[33] Belov, Sov. Phys. Crystallogr. **2,** 311 (1957).

[34] B. J. Campbell, H. T. Stokes, D. E. Tanner, and D. M. Hatch, ISODISPLACE: a web-based tool for exploring structural distortions, J. Appl. Crystallogr. **39,** 607 (2006).

[35] We have used the program CrysCalCon distributed within the FullProf Suite for calculating the expected ionic polarization per unit volume assuming formal charges and the experimental structural data.

[36] See Supplemental Material for detailed structural analysis on $R FeWO_6$ (R = Eu, Tb and Y).

Figure Captions:

Figure 1 (a, b) Results of combined Rietveld refinement of room temperature synchrotron X - ray and neutron diffraction data. (c) The aeschynite-type crystal structure of $CaTa_2O_6$. (d) The ordered aeschynite-type crystal structure of $DyFeWO_6$.

Figure 2 (a) Temperature dependence of field - cooled magnetization of $DyFeWO_6$ under a magnetic field of 100 Oe. The inset shows magnetic field dependent magnetization at different temperatures. (b) Temperature dependent heat capacity (C_P) of $DyFeWO_6$.

Figure 3 (a) Results of Rietveld refinement of neutron diffraction data of $DyFeWO_6$ collected at 3.5 K. The first row of vertical bars represents the nuclear Bragg positions and second row represents magnetic Bragg peak positions. (b) The magnetic structure of $DyFeWO_6$.

Figure 4 (a) Temperature variation of the real part of dielectric constant $\varepsilon'(T)$ of $DyFeWO_6$ measured with different frequencies. The inset shows the corresponding imaginary part of the dielectric constant $\varepsilon''(T)$. (b) Temperature dependence of the real part of dielectric constant $\varepsilon'(T)$ at 50 kHz measured in the presence of different applied magnetic fields.

Figure 5 (a) Temperature evolution of electric polarization ΔP (T) of $DyFeWO_6$ below T_N^{Fe} = 18 K obtained from pyroelectric current measurements under an electric field of E = ± 9.2 kV/cm and different magnetic fields. The inset shows magnetic field - dependent change in electric polarization measured at 10 K with ramping magnetic field with a rate of 120 Oe/sec after poling the sample with an electric field of E = + 9.2 kV/cm. (b) Temperature - dependence of dc-biased current of $DyFeWO_6$ measured with an electric field of E_{dc} = + 9.2 kV/cm and magnetic fields of 0 kOe and 40 kOe.

Figure 6 (a) Variation of FC magnetization M (T) with temperature under a magnetic field of 100 Oe in $EuFeWO_6$. The inset shows magnetization *vs.* magnetic field data measured at 2 K. (b) Temperature dependent heat capacity (C_P) of $EuFeWO_6$. (c) Temperature variation of the real part of dielectric constant ε' (T) of $EuFeWO_6$ measured with 50 kHz under different magnetic fields. (d) Evolution of electric polarization ΔP (T) with temperature below T_N^{Fe} in $EuFeWO_6$ obtained from pyroelectric current measurements with an electric field of E = + 7.7 kV/cm and different magnetic fields.

Figure 7 (a) Temperature dependent FC magnetization M (T) of $TbFeWO_6$ measured under a magnetic field of 100 Oe. Inset shows the magnetic field dependence of magnetization measured at different temperatures. (b) Temperature variation of heat capacity C_P (T) of $TbFeWO_6$. (c) Temperature dependence of the real part of the dielectric constant ε' (T) measured with 50 kHz under different magnetic fields. (d) Electric polarization ΔP (T) measured with an electric field of E = + 5.8 kV/cm and different applied magnetic fields.

Figure 8 (a) Temperature variation of magnetization of $YFeWO_6$ measured with a magnetic field of 100 Oe under field - cooled condition. M (H) loop measured at 2 K is shown in the inset. (b) Temperature dependence of C_P (T). (c, d) Temperature evolution of dielectric constant ε' (T) and electric polarization ΔP (T) measured with different magnetic fields in $YFeWO_6$.

Tables:

Tables I Crystallographic parameters of $DyFeWO_6$ obtained from combined Rietveld refinement of room temperature synchrotron X-ray (λ = 0.3544 Å) and neutron diffraction data

Atom	Wyckoff position	*x*	*y*	*z*	B_{iso} (Å^2)	Occ.
Dy	4*a*	0.0426(1)	0.4570(2)	0.25	0.49(1)	1
Fe	4*a*	0.1378(2)	0.9661(5)	0.9925(5)	0.80(4)	1
W	4*a*	0.3539(1)	0.4519(2)	0.0057(3)	0.13(1)	1
O1	4*a*	0.9703(7)	0.7683(15)	0.0424(14)	0.77(17)	1
O2	4*a*	0.5221(7)	0.2542(16)	0.9610(15)	0.99(19)	1
O3	4*a*	0.2130 (8)	0.6145(19)	0.0622 (15)	1.24(19)	1
O4	4*a*	0.2919(8)	0.1278(17)	0.9333(13)	0.68(16)	1
O5	4*a*	0.1437(3)	0.0590(7)	0.2583(16)	0.94(6)	1
O6	4*a*	0.1197(3)	0.8289(6)	0.7500 (20)	0.83(6)	1

Space group: $Pna2_1$; a = 10.97992 (2) Å, b = 5.18849(1) Å, c = 7.34824(1) Å, $\alpha = \beta = \gamma = 90°$, V = 418.624(1) Å^3; χ^2 = 1.75 (for neutron), χ^2 = 1.07 (for synchrotron); Bragg R-factor = 3.66, R_f-factor = 2.36 (for neutron); Bragg R-factor = 3.67, R_f-factor = 2.80 (for synchrotron)

Tables II Selected bond lengths (Å) and bond valence sum (BVS) of $DyFeWO_6$ at room temperature

Cation	O1	O2	O3	O4	O5	O6
Dy	2.36(1) 2.45(1)	2.30(1) 2.40(1)	2.46(1)	2.43(1)	2.34(0)	2.32(0)
Fe	2.14(1)	1.94(1)	2.07(1)	1.94(1)	2.01(1)	1.93(1)
W	1.95(1)	2.14(1)	1.81(1)	1.89(1)	1.90 (1)	1.93(1)
BVS Dy				2.88(2)		
BVS Fe				3.15(4)		
BVS W				5.88(7)		

Tables III Crystallographic parameters of $DyFeWO_6$ at 3.5 K obtained from Rietveld refinement of neutron diffraction data. Ordered magnetic moments at different temperatures are shown at the bottom rows.

a = 10.97334(11) Å, b = 5.18423(5) Å, c = 7.33767(7) Å, $\alpha = \beta = \gamma = 90°$, V = 417.427(7) Å^3, χ^2 = 2.25; Bragg R-factor = 2.22, R_f-factor = 1.22

Name	**Wyckoff position**	***x***	***y***	***z***	B_{iso} **(Å^2)**	**Occ.**
Dy	4*a*	0.0424(1)	0.4576(2)	0.25	0.43(2)	1
Fe	4*a*	0.1363(4)	0.9642(10)	0.9936(10)	0.86(9)	1
W	4*a*	0.3530(6)	0.4572(16)	0.0095(15)	0.07(13)	1
O1	4*a*	0.9732(7)	0.7639(15)	0.0385(17)	0.23(14)	1
O2	4*a*	0.5234(10)	0.2579(20)	0.9550(22)	1.48(22)	1
O3	4*a*	0.2151(8)	0.6088(19)	0.0630(14)	1.47(20)	1
O4	4*a*	0.2938(6)	0.1290(13)	0.9342(11)	0.11(13)	1
O5	4*a*	0.1437(3)	0.0593(7)	0.2522(24)	0.83(5)	1
O6	4*a*	0.1204(3)	0.8290(6)	0.7466(20)	0.56(6)	1

Ordered magnetic moments

T **(K)**	$\mu_{Dy^{3+}}(\mu_B)$	$\mu_{Fe^{3+}}(\mu_B)$
3.5	7.90(4)	4.48(9)
10	5.71(6)	4.29(12)
15	3.57(9)	3.87(17)

Figure 1

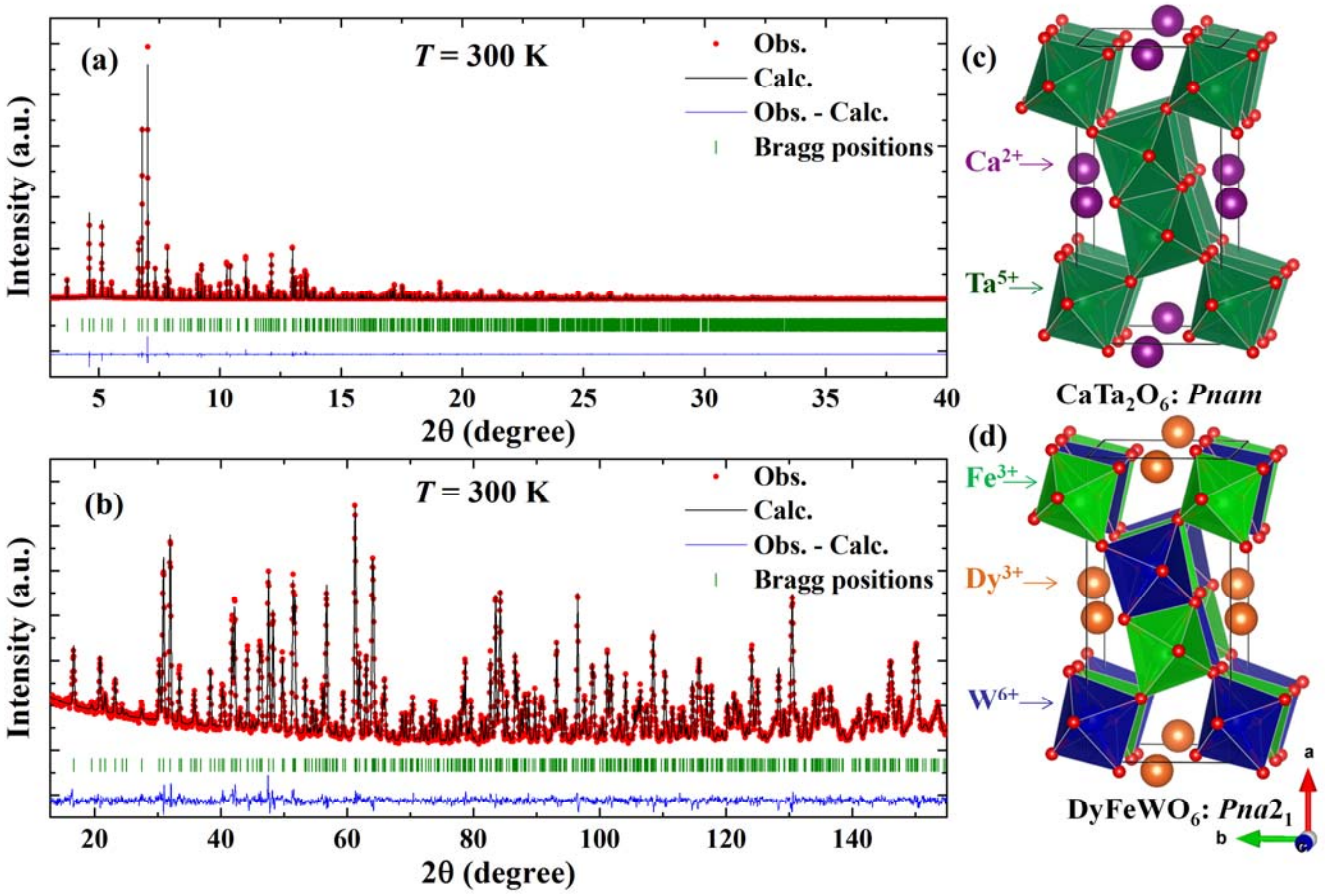
(a)
T = 300 K
Obs.
Calc.
Obs. - Calc.
Bragg positions
Intensity (a.u.)
2θ (degree)
(b)
T = 300 K
Obs.
Calc.
Obs. - Calc.
Bragg positions
Intensity (a.u.)
2θ (degree)
(c)
Ca2+
Ta5+
CaTa2O6: Pnam
(d)
Fe3+
Dy3+
W6+
a
b
DyFeWO6: Pna21

Figure 2

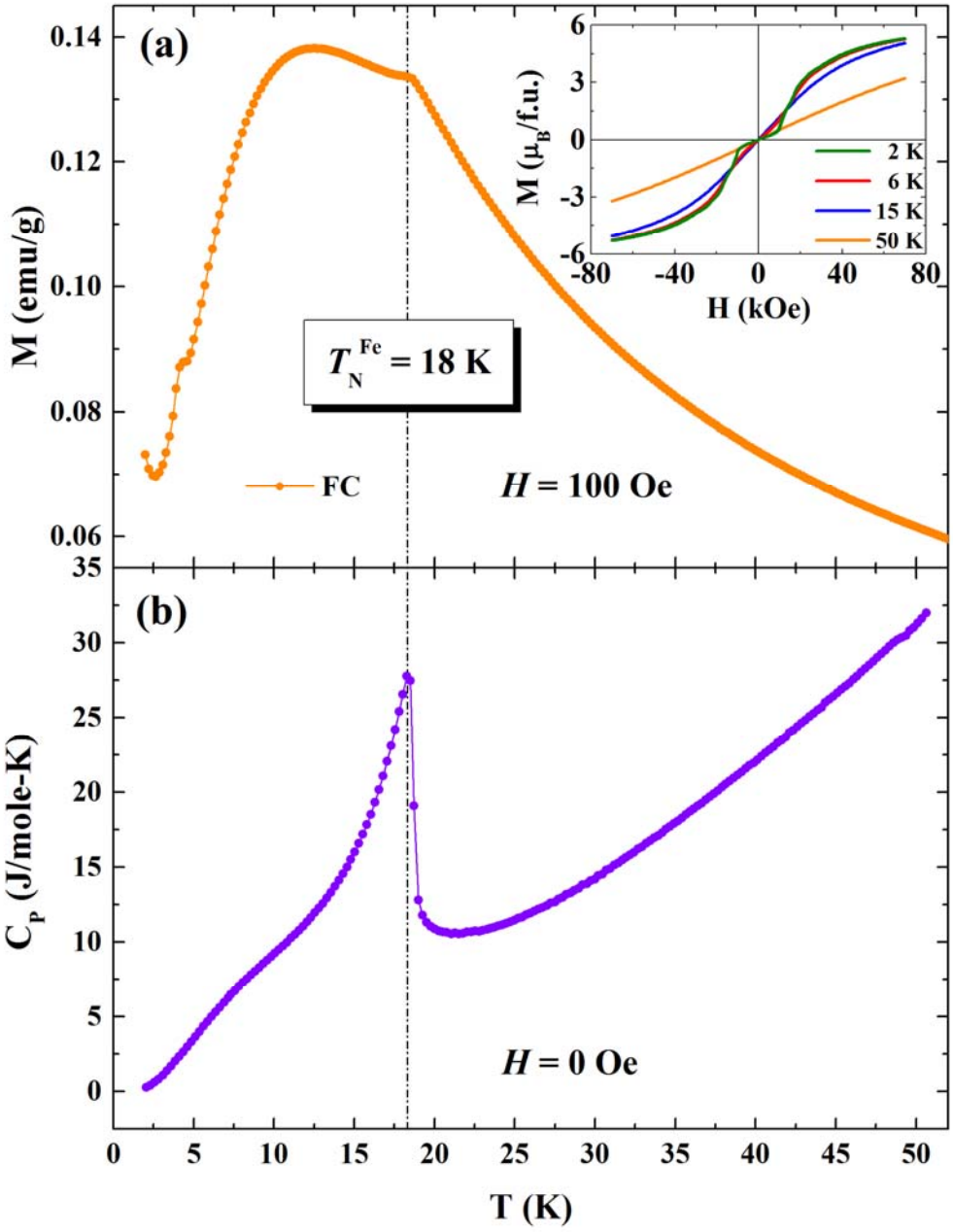
(a)
0.14
0.12
0.10
0.08
0.06
M (emu/g)
T_N^{Fe} = 18 K
FC
H = 100 Oe
6
3
0
-3
-6
M (μ_B/f.u.)
2 K
6 K
15 K
50 K
-80
-40
0
40
80
H (kOe)
(b)
35
30
25
20
15
10
5
0
C_P (J/mole-K)
H = 0 Oe
0
5
10
15
20
25
30
35
40
45
50
T (K)

Figure 3

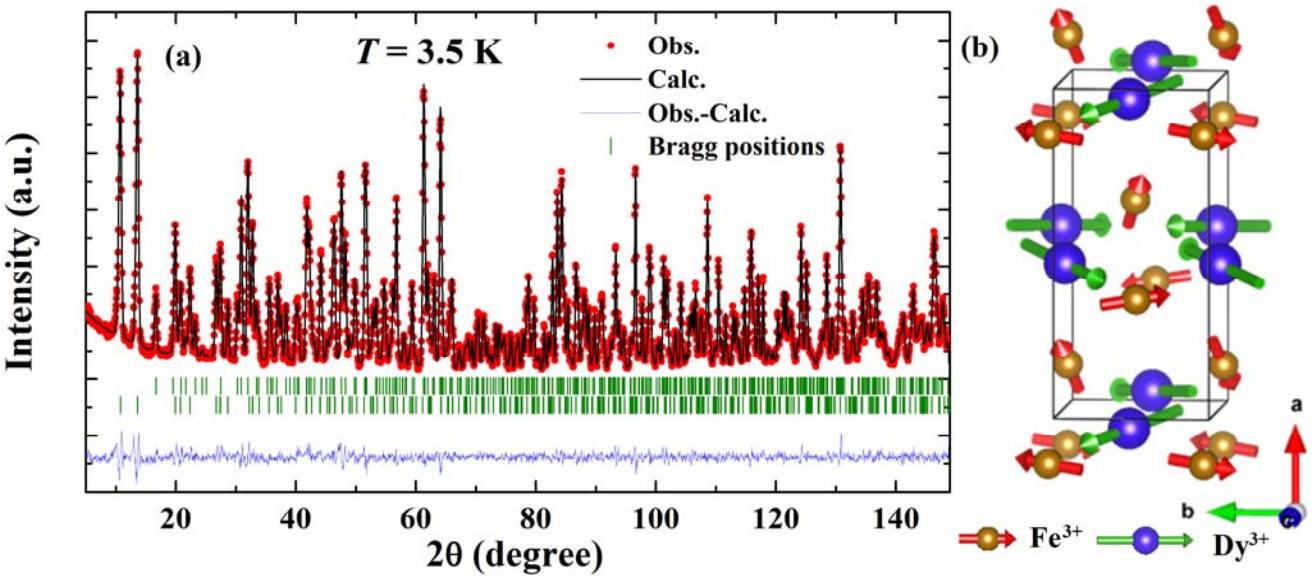
(a)
T = 3.5 K
Obs.
Calc.
Obs.-Calc.
Bragg positions
Intensity (a.u.)
20
40
60
80
100
120
140
2θ (degree)
(b)
a
b
c
Fe3+
Dy3+

Figure 4

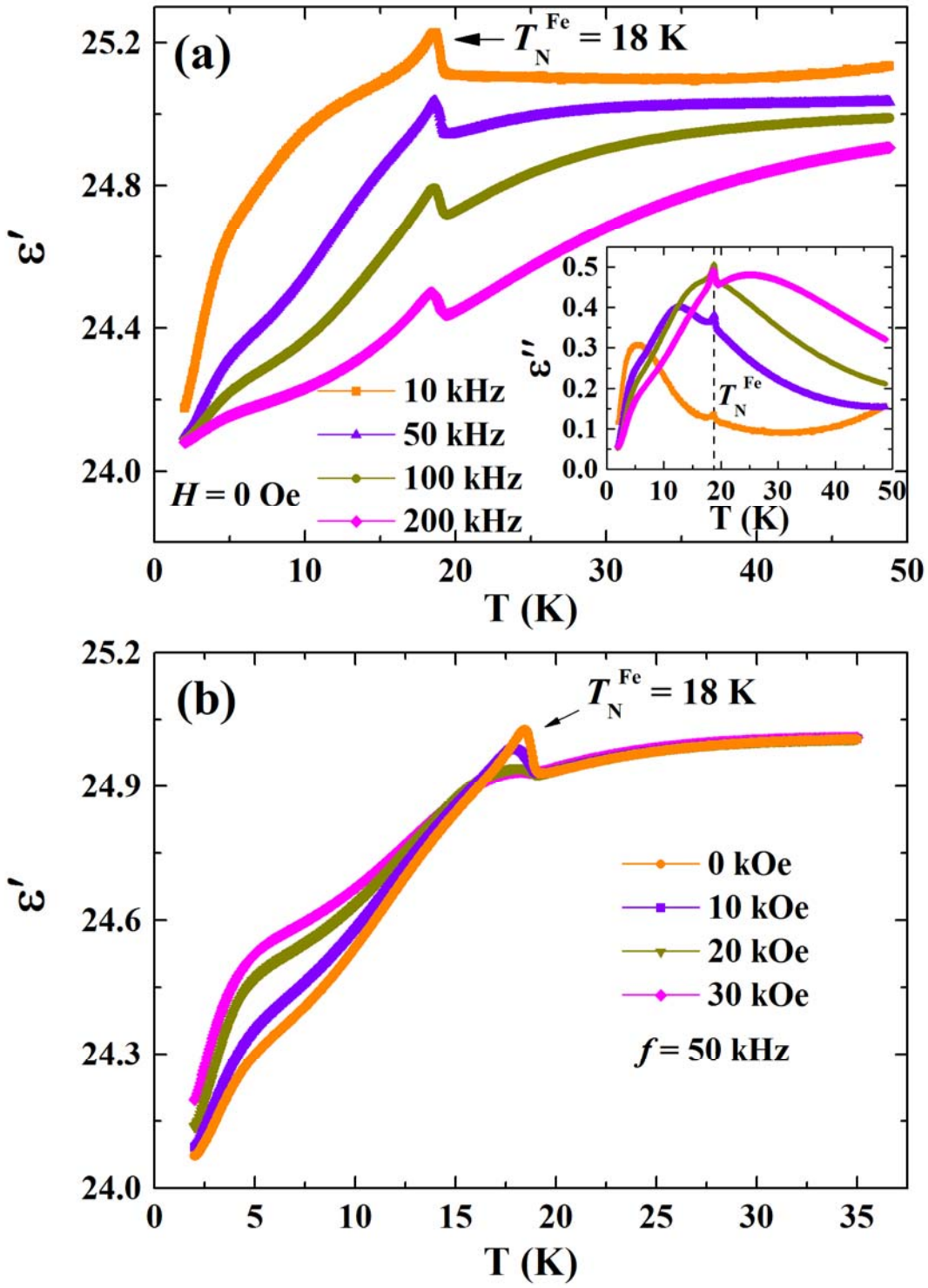
(a)
T_N^{Fe} = 18 K
25.2
24.8
24.4
24.0
ε′
0
10
20
30
40
50
T (K)
10 kHz
50 kHz
100 kHz
200 kHz
H = 0 Oe
ε″
0.5
0.4
0.3
0.2
0.1
0.0
T_N^{Fe}
(b)
T_N^{Fe} = 18 K
24.9
24.6
24.3
24.0
0
5
10
15
20
25
30
35
0 kOe
10 kOe
20 kOe
30 kOe
f = 50 kHz

Figure 5

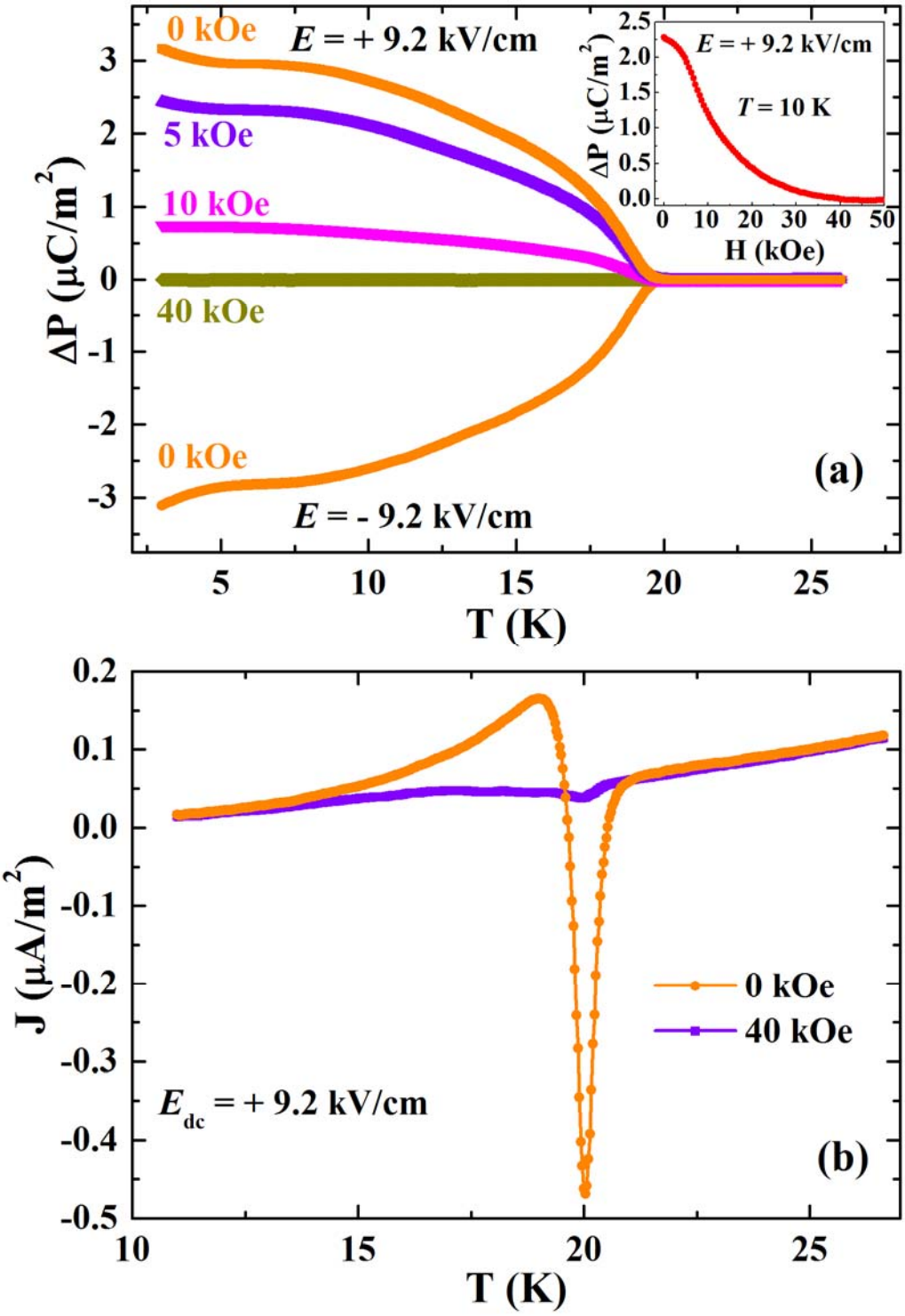
0 kOe
E = + 9.2 kV/cm
5 kOe
10 kOe
40 kOe
0 kOe
E = - 9.2 kV/cm
(a)
ΔP (μC/m²)
T (K)
E = + 9.2 kV/cm
T = 10 K
ΔP (μC/m²)
H (kOe)
E_dc = + 9.2 kV/cm
0 kOe
40 kOe
(b)
J (μA/m²)
T (K)

Figure 6

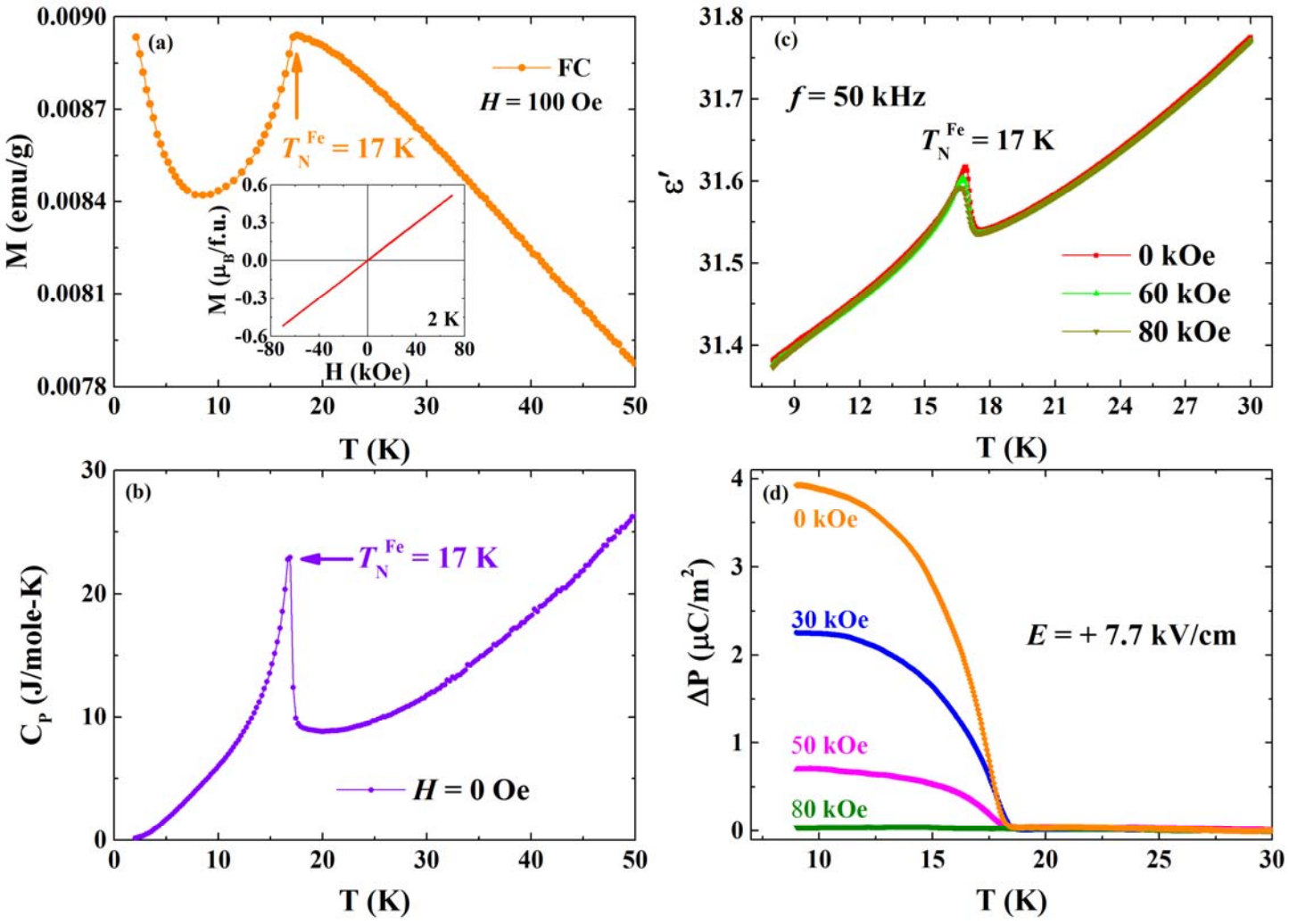
(a)
FC
H = 100 Oe
T_N^{Fe} = 17 K
M (emu/g)
T (K)
M (μ_B/f.u.)
H (kOe)
2 K
(b)
T_N^{Fe} = 17 K
H = 0 Oe
C_P (J/mole-K)
T (K)
(c)
f = 50 kHz
T_N^{Fe} = 17 K
ε′
0 kOe
60 kOe
80 kOe
T (K)
(d)
0 kOe
30 kOe
50 kOe
80 kOe
E = + 7.7 kV/cm
ΔP (μC/m²)
T (K)

Figure 7

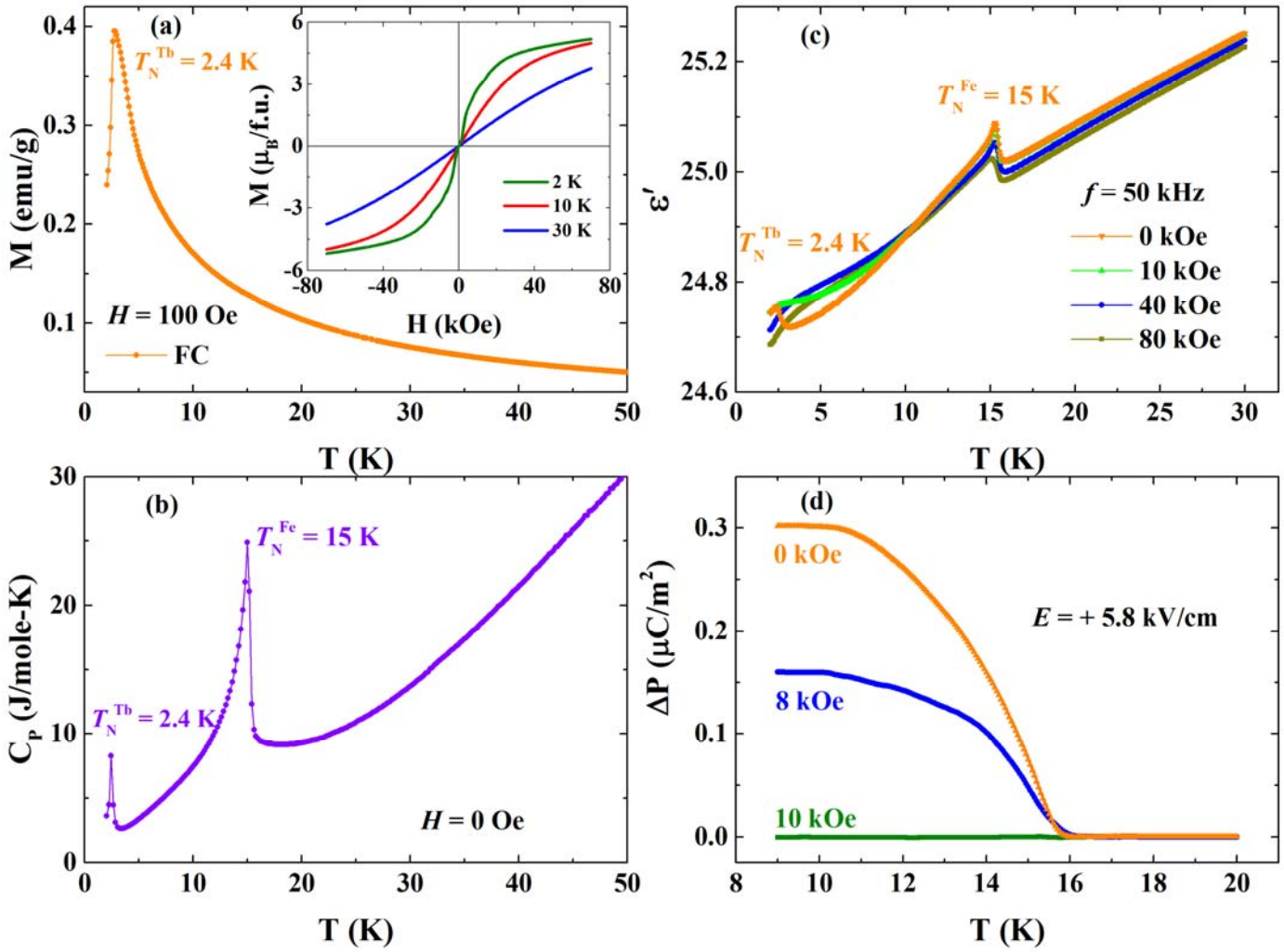
(a)
T_N^{Tb} = 2.4 K
M (emu/g)
H = 100 Oe
FC
T (K)
M (μ_B/f.u.)
2 K
10 K
30 K
H (kOe)
(b)
T_N^{Fe} = 15 K
T_N^{Tb} = 2.4 K
C_p (J/mole-K)
H = 0 Oe
T (K)
(c)
T_N^{Fe} = 15 K
T_N^{Tb} = 2.4 K
ε′
f = 50 kHz
0 kOe
10 kOe
40 kOe
80 kOe
T (K)
(d)
0 kOe
8 kOe
10 kOe
E = + 5.8 kV/cm
ΔP (μC/m^2)
T (K)

Figure 8

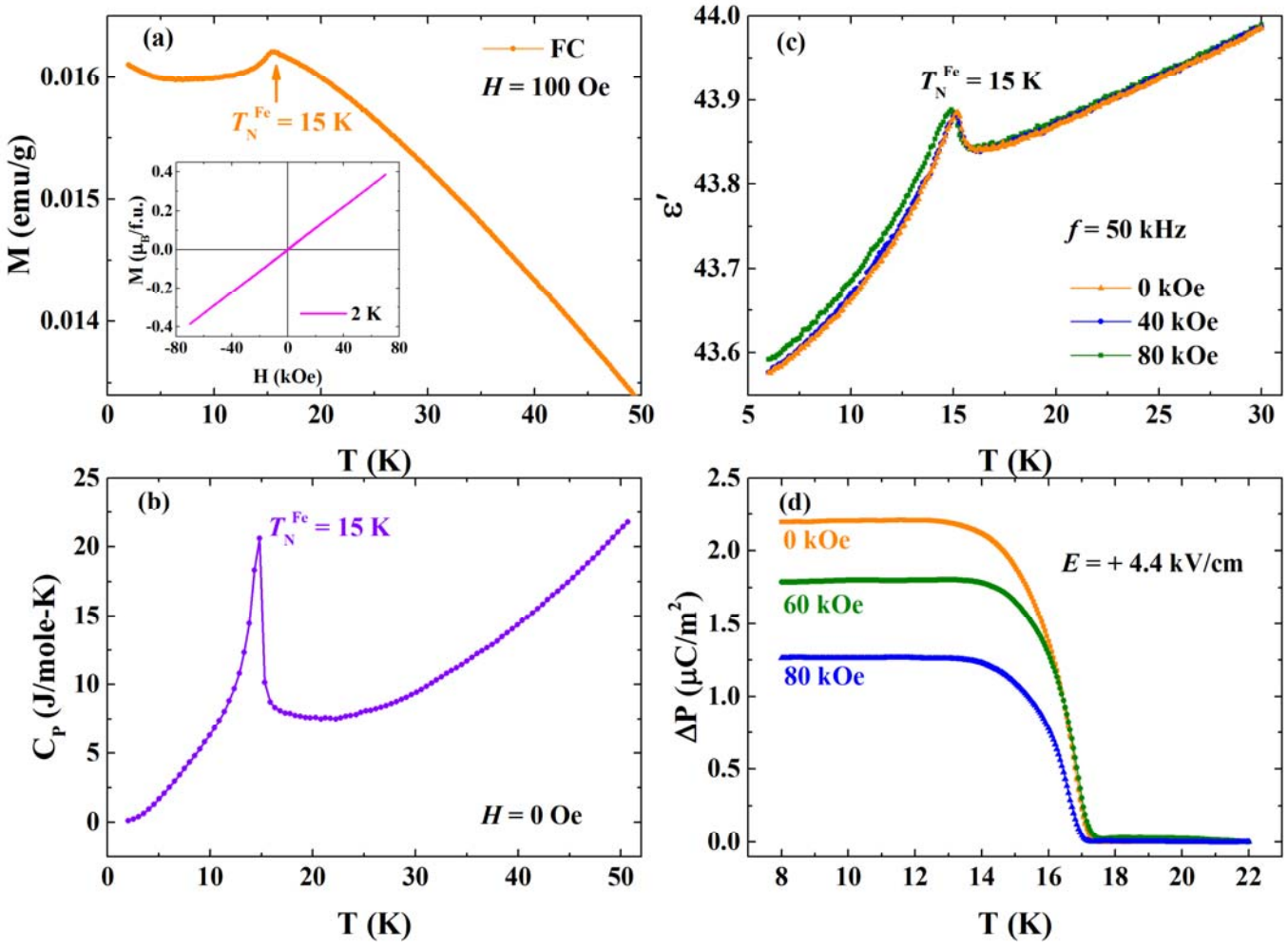
(a)
FC
H = 100 Oe
T_N^{Fe} = 15 K
M (emu/g)
T (K)
M (μ_B/f.u.)
H (kOe)
2 K
(b)
T_N^{Fe} = 15 K
H = 0 Oe
C_p (J/mole-K)
T (K)
(c)
T_N^{Fe} = 15 K
f = 50 kHz
0 kOe
40 kOe
80 kOe
ε′
T (K)
(d)
0 kOe
60 kOe
80 kOe
E = + 4.4 kV/cm
ΔP (μC/m²)
T (K)